Hydrogen production by auto-thermal reforming of ethanol over nickel catalysts supported on metal oxides: Effect of support acidity

Min Hye Youn [a], Jeong Gil Seo [a], Howon Lee [a], Yongju Bang [a], Jin Suk Chung [b], In Kyu Song [a,*]

[a] School of Chemical and Biological Engineering, Institute of Chemical Processes, Seoul National University, Shinlim-dong, Kwanak-ku, Seoul 151-744, Republic of Korea
[b] School of Chemical Engineering and Bioengineering, University of Ulsan, Ulsan 680-749, Republic of Korea

ARTICLE INFO

ABSTRACT

Nickel catalysts supported on pure metal oxides (ZnO, MgO, ZrO_2, TiO_2, and Al_2O_3) with different acidity were prepared by an incipient wetness impregnation method, and they were applied to the hydrogen production by auto-thermal reforming of ethanol. The effect of support acidity on the catalytic performance of supported nickel catalysts was investigated. It was revealed that acidity of support played an important role in determining the reaction pathway and catalytic performance in the auto-thermal reforming of ethanol. Among various pure metal oxides, ZrO_2 and TiO_2 with an intermediate acidity were found to be efficient supporting materials for nickel catalysts in the auto-thermal reforming of ethanol. On the basis of this result, a series of TiO_2–ZrO_2 mixed metal oxides ($Ti_X Zr_{1-X}O_2$) with different Ti content (X) were prepared by a sol–gel method for use as supporting materials for nickel catalysts. In hydrogen production by auto-thermal reforming of ethanol, an optimal Ti content was required for suitable acidity of $Ti_X Zr_{1-X}O_2$ support and favorable reducibility of $Ni/Ti_X Zr_{1-X}O_2$ catalyst. Hydrogen yield over nickel catalysts supported on metal oxides showed a volcano-shaped curve with respect to acidity of the support. Among the catalysts tested, $Ni/Ti_{0.2}Zr_{0.8}O_2$ with an intermediate acidity of support exhibited the best catalytic performance.

1. Introduction

With increasing concern about global warming and fossil fuel depletion, a demand for development of new and clean energy has increased dramatically [1]. Current energy needs are majorly supplied by combustion of fossil fuels which has caused severe environmental problems such as toxic gas and particulate emissions [2]. In addition, many unusual weather phenomena attributed to global warming suggest that an alternative renewable energy source to overcome these obstacles of fossil fuels is urgently needed.

In this respect, hydrogen is considered to be the most viable energy carrier due to its clean and non-polluting nature [3]. In particular, technological advances in hydrogen utilization such as fuel cells make hydrogen more important as a new fuel [4]. In recent years, considerable efforts have been made in developing processes for hydrogen production from renewable biomass sources [5]. Among renewable energy sources for hydrogen production, ethanol has served as a promising source because it can be easily handled and is widely distributed around the world. In addition, its low toxicity and high volumetric energy density also make it an attractive energy source for hydrogen production [6].

Several catalytic processes for hydrogen production from ethanol have been investigated, including steam reforming, partial oxidation, and auto-thermal reforming [7]. Among these catalytic reforming technologies, auto-thermal reforming has many advantages in terms of heat management and reforming efficiency [8]. Although noble metals are highly active in the auto-thermal reforming reactions, nickel-based catalysts have also been widely used in the reforming processes due to their high intrinsic activity and low cost [7,9]. Auto-thermal reforming of ethanol over supported nickel catalysts has been studied by several research groups [10–15]. Typical nickel-based catalysts examined for auto-thermal reforming of ethanol include Ni/CeO_2 [10], Ni/CeO_2–ZrO_2 [11], Ni–Rh/CeO_2 [12], Ni/MgO [13], Ni/ZrO_2 [14], and Ni–Mo/Al_2O_3 [15].

In general, the identity of support strongly affects the catalytic performance of supported nickel catalysts in the catalytic reforming reactions [16–19]. Supports also promote migration of OH group toward metal catalyst in the presence of water at high temperature, facilitating catalytic reforming reactions [20]. In particular, acidity of support is one of the important factors determining the catalytic performance of supported nickel catalysts in the auto-thermal reforming reactions [21,22].

* Corresponding author. Tel.: +82 2 880 9227; fax: +82 2 889 7415.
  E-mail address: inksong@snu.ac.kr (I.K. Song).

In this work, nickel catalysts supported on various pure metal oxides (ZnO, MgO, ZrO₂, TiO₂, and Al₂O₃) were prepared by an incipient wetness impregnation method for use in hydrogen production by auto-thermal reforming of ethanol. In addition, a series of $Ti_XZr_{1-X}O_2$ mixed metal oxides with different Ti content were synthesized by a sol–gel method. $Ni/Ti_XZr_{1-X}O_2$ catalysts were then prepared by an incipient wetness impregnation method, and they were applied to the hydrogen production by auto-thermal reforming of ethanol. The prepared catalysts were characterized by SEM-EDX, BET, XRD, TPR, TEM, and TPD analyses to elucidate their catalytic performance. The effect of support acidity on the catalytic performance of supported nickel catalysts in the auto-thermal reforming of ethanol was investigated.

2. Experimental

2.1. Preparation of supported nickel catalysts

A series of supported nickel catalysts were prepared by impregnating appropriate amount of nickel precursor ($Ni(NO_3)_2·6H_2O$) onto commercial ZnO, MgO, ZrO₂, TiO₂, and Al₂O₃. The impregnated catalysts were dried at 120 °C, and then they were calcined at 550 °C for 5 h. Nickel loading was fixed at 20 wt% [17,23].

TiO₂–ZrO₂ mixed metal oxides with different Ti content were prepared by a sol–gel method for use as supporting materials for nickel catalysts. Known amounts of zirconium butoxide ($Zr(OBu)_4$, Sigma–Aldrich) and titanium butoxide ($Ti(OBu)_4$, Sigma–Aldrich) were separately dissolved in 2-butanol ($C_4H_{10}O$, Sigma–Aldrich). A small amount of acetylacetone ($C_5H_8O_2$, Sigma–Aldrich) was added into a solution containing zirconium precursor, with an aim of controlling the hydrolysis rate. These two solutions containing metal precursors were then mixed with vigorous stirring to form a single solution, and pH of the resulting solution was adjusted at 9 by adding an appropriate amount of aqueous ammonia solution (30%, Sigma–Aldrich). A known amount of distilled water was added dropwise into the mixed solution to form a gel. The obtained product was washed with distilled water and filtered. It was then dried at 80 °C in a convection oven to obtain a solid. The solid product was finally calcined at 550 °C for 5 h to yield a TiO₂–ZrO₂ mixed metal oxide. TiO₂–ZrO₂ mixed metal oxides with different Ti content (X) were denoted as $Ti_XZr_{1-X}O_2$ (X = 0, 0.2, 0.5, 0.8, and 1). Nickel catalysts supported on $Ti_XZr_{1-X}O_2$ (X = 0, 0.2, 0.5, 0.8, and 1) were prepared by an incipient wetness impregnation method. The supported nickel catalysts were dried at 120 °C, and subsequently, they were calcined at 550 °C for 5 h. The prepared catalysts were denoted as $Ni/Ti_XZr_{1-X}O_2$ (X = 0, 0.2, 0.5, 0.8, and 1). Nickel loading on $Ti_XZr_{1-X}O_2$ was fixed at 20 wt% [17,23].

2.2. Characterization

Acidities of various metal oxide supports were measured by NH₃-TPD experiments. Each support (0.1 g) was charged into a tubular quartz reactor of the conventional TPD apparatus. The catalyst was pretreated at 200 °C for 1 h under a flow of helium (20 ml/min) to remove any physisorbed organic molecules. Twenty milliliters of ammonia gas was then pulsed into the reactor every minute at room temperature under a flow of helium (5 ml/min), until acid sites were saturated with ammonia. Physisorbed ammonia was removed by evacuating the catalyst sample at 50 °C for 1 h. Furnace temperature was increased from room temperature to 700 °C at a heating rate of 10 °C/min under a flow of helium (10 ml/min). The desorbed ammonia was detected using a GC-MSD (Agilent, MSD-6890N GC). Chemical compositions of $Ti_XZr_{1-X}O_2$ (X = 0, 0.2, 0.5, 0.8, and 1) supports were determined by SEM-EDX (Jeol, JSM-6700F) analyses. Surface areas of $Ti_XZr_{1-X}O_2$ supports

were measured using a BET apparatus (Micromeritics, ASAP 2010). Crystalline phases of calcined and reduced catalysts were determined by XRD (MAC Science, M18XHF-SRA) measurements using Cu Kα radiation (λ = 1.54056 Å) operated at 50 kV and 100 mA. TEM analyses (JEM-2000EXII, JEOL) were conducted to examine the nickel dispersion on the reduced catalysts. In order to check the reducibility of the catalysts, temperature-programmed reduction (TPR) measurements were carried out in a conventional flow system with a moisture trap connected to a thermal conductivity detector at temperatures ranging from room temperature to 1000 °C with a ramping rate of 5 °C/min. For the TPR measurements, a mixed stream of H₂ (2 ml/min) and N₂ (20 ml/min) was used for 0.1 g of catalyst sample.

2.3. Auto-thermal reforming of ethanol

Auto-thermal reforming of ethanol was carried out in a continuous flow fixed-bed reactor at atmospheric pressure. Each calcined catalyst (50 mg) was charged into a tubular quartz reactor, and then it was reduced with a mixed stream of H₂ (10 ml/min) and N₂ (30 ml/min) at 500 °C for 2 h. Ethanol and water were sufficiently vaporized by passing through a pre-heating zone, and were continuously fed into the reactor together with N₂ carrier (30 ml/min). Feed ratios of H₂O/EtOH and O₂/EtOH were fixed at 3.0 and 0.5, respectively. Contact time was maintained at 175 g-catalyst min/EtOH-mol. Catalytic reaction was carried out at 500 °C. Reaction products were periodically sampled and analyzed using an on-line gas chromatograph (Younglin, ACME 6000) equipped with a thermal conductivity detector. Reactant conversion, product selectivity, and H₂ yield were calculated according to the following equations. Here, n represents the number of moles and χ is a stoichiometry factor (χ = 2 for C₁, χ = 1 for C₂, and χ = 2/3 for C₃ compounds):

$$\text{Reactant conversion} = \frac{(n_{\text{Reat, in}} - n_{\text{Reat, out}})}{n_{\text{Reat, in}}} \times 100 \tag{1}$$

$$\text{H}_2 \text{ selectivity} = \frac{n_{\text{H}_2}}{3(n_{\text{EtOH, in}} - n_{\text{EtOH, out}}) + (n_{\text{H}_2\text{O, in}} - n_{\text{H}_2\text{O, out}})} \times 100 \tag{2}$$

$$\text{C}_\chi \text{ selectivity} = \frac{n_{\text{C}_\chi}}{\chi(n_{\text{EtOH, in}} - n_{\text{EtOH, out}})} \times 100 \tag{3}$$

$$\text{H}_2 \text{ yield} = \frac{n_{\text{H}_2}}{n_{\text{EtOH,in}}} \tag{4}$$

3. Results and discussion

3.1. Acidity of various pure metal oxide supports

To investigate the effect of support identity on the catalytic performance of supported nickel catalysts, a series of nickel catalysts supported on commercial metal oxides such as ZnO, MgO, ZrO₂, TiO₂, and Al₂O₃ were prepared by an incipient wetness impregnation method, and they were applied to the hydrogen production by auto-thermal reforming of ethanol. Among various properties of supporting materials, it is known that acidity of support plays an important role in determining the reaction mechanism and catalytic performance of supported nickel catalyst [21–24]. In order to determine the acidity of various pure metal oxide supports, NH₃-TPD experiments were conducted. Fig. 1 shows the NH₃-TPD profiles of various pure metal oxide supports. Acidity of supports determined from TPD peak area increased in the order of MgO
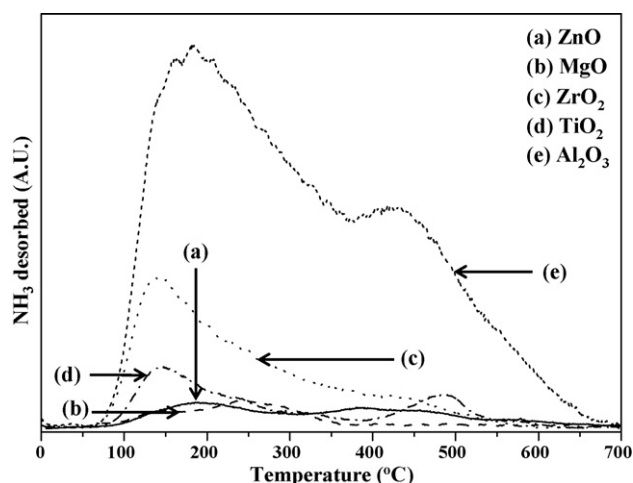
Fig. 1. NH_3-TPD profiles of various pure metal oxide supports.

Table 1
Possible reaction pathways for auto-thermal reforming of ethanol.

Reaction	ΔH_{298}° (kJ/mol)
$C_2H_5OH + 2H_2O + 1/2O_2 \rightarrow 2CO_2 + 5H_2$	−68
$C_2H_5OH + 3H_2O \rightarrow 2CO_2 + 6H_2$	174
$C_2H_5OH + 1/2O_2 \rightarrow 2CO + 3H_2$	14
$C_2H_5OH + 3O_2 \rightarrow 2CO_2 + 3H_2O$	−1277
$C_2H_5OH + H_2O \rightarrow 2CO + 4H_2$	256
$C_2H_5OH + 2H_2 \rightarrow 2CH_4 + H_2O$	−157
$C_2H_5OH \rightarrow CH_3CHO + H_2$	68
$C_2H_5OH \rightarrow C_2H_4 + H_2O$	45
$C_2H_5OH \rightarrow 1/2CO_2 + 2/3CH_4$	−74
$C_2H_5OH \rightarrow CO + CH_4 + H_2$	49
$2CO \rightarrow CO_2 + C$	−171.5
$C_2H_4 \rightarrow$ polymers $\rightarrow$ coke	
$CH_4 + H_2O \rightarrow CO + 3H_2$	205
$CO + H_2O \rightarrow CO_2 + H_2$	−41.2
$CO + 1/2O_2 \rightarrow CO_2$	−283.3
$C_2H_5OH + 1/2O_2 \rightarrow CH_3CHO + H_2O$	−203.3
$CH_4 + 2O_2 \rightarrow CO_2 + 2H_2O$	−212.9
$C + O_2 \rightarrow CO_2$	−393.5
$CH_3CHO + H_2O \rightarrow CO_2 + CH_4 + H_2$	−55.8
$C_2H_4 + 2H_2O \rightarrow CO_2 + CH_4 + 2H_2$	−36.9

(84.0 μmol-NH_3/g) < ZnO (123.4 μmol-NH_3/g) < TiO_2 (284.1 μmol-NH_3/g) < ZrO_2 (420.5 μmol-NH_3/g) < Al_2O_3 (1693.1 μmol-NH_3/g).

3.2. Catalytic performance of nickel catalysts supported on various pure metal oxides

It is known that ethanol reforming reaction for hydrogen production is strongly linked to several side reactions. Possible reaction pathways for auto-thermal reforming of ethanol are summarized in Table 1. Fig. 2 shows the ethanol conversion and water conversion over various pure metal oxide supports and supported nickel catalysts in the auto-thermal reforming of ethanol at 500 °C. Ethanol conversion reached more than 80% over all metal oxide supports. Ethanol conversion over pure metal oxide supports increased in the order of MgO (85.9%) < ZnO (87.8%) < TiO_2 (93.5%) < ZrO_2 (94.3%) < Al_2O_3 (99.8%), in good agreement with the trend of support acidity (Fig. 1). Unlike metal oxide supports, all the supported nickel catalysts showed complete conversion of ethanol. As shown in Fig. 2(b), on the other hand, pure metal oxide supports exhibited water conversion of less than 5%, except for ZrO_2 and TiO_2. It has been reported that ZrO_2 and TiO_2, which are known as easily reducible metal oxide, have ability to adsorb and dissociate water [25–27]. Although water conversion over supported nickel catalysts was higher than that over supports, it was obvious that water conversion over supported nickel catalyst was strongly influenced by the identity of supporting material. This is because nickel catalyst facilitated ethanol consumption and promoted water consumption in the reaction. Among the supports and supported nickel

catalysts tested, ZrO_2 support and Ni/ZrO_2 catalyst exhibited an excellent water conversion. This result is in good agreement with the previous work [28,29] reporting that zirconia support enhanced adsorption of steam onto its surface and activated gasification of hydrocarbons or carbon precursors adsorbed on the catalyst surface in the steam reforming reactions. It is known that hydrogen production by reforming process over Ni catalyst is closely related to the adsorption mechanisms of dissociate hydrocarbon and steam [28]. Adsorption of steam takes place competitively on the nickel and support, and zirconia is known to have a high capacity for steam adsorption. Zirconia also plays an important role in enhancing the spillover of adsorbed steam from the support to the active nickel. The migrated steam, in turn, enhances the gasification of surface hydrocarbons or carbon species, resulting in enhanced hydrogen production [29].

Table 2 shows the product selectivities over various pure metal oxide supports and supported nickel catalysts. Over ZnO and MgO supports with weak/low acidity, CH_3CHO, CH_3COCH_3, and CH_3COOH were mainly produced as by-products. In other words, weak/low acidity of ZnO and MgO supports favorably served to promote ethanol dehydrogenation reaction. In case of Al_2O_3 with strong/high acidity, however, C_2H_4 and C_2H_6 were mainly produced. It has been generally accepted that acidic support induces ethanol dehydration to produce ethylene which acts as a source of coke formation. The above result strongly suggests that support acidity plays a key role in determining the reaction pathway
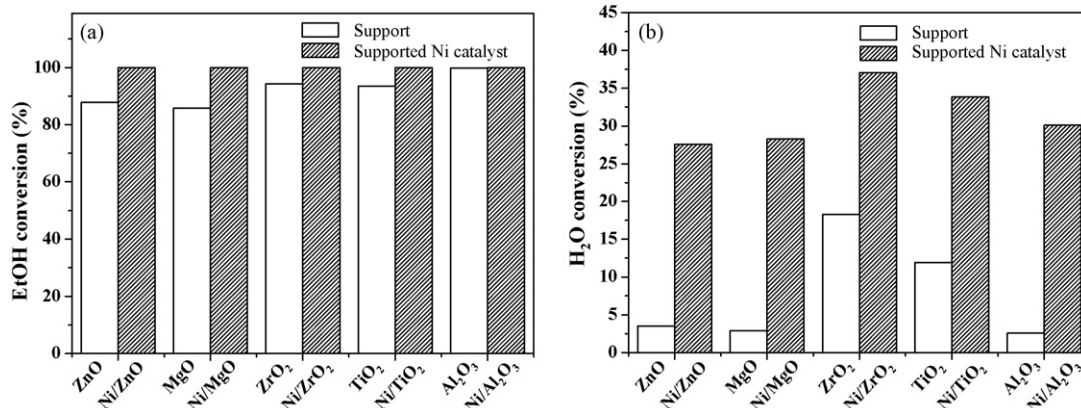

Fig. 2. (a) Ethanol conversion and (b) water conversion over various pure metal oxide supports and supported nickel catalysts.

Table 2
Product selectivities over various pure metal oxide supports and supported nickel catalysts.

	H_2	CO	CO_2	CH_4	CH_3CHO	C_2H_4	C_2H_6	CH_3COCH_3	CH_3COOH
ZnO	20.9	0.6	11.5	7.6	45.4	1.5	2.6	18.4	12.5
Ni/ZnO	45.3	5.4	38.4	47.3	8.5	0.0	0.0	1.4	0.0
MgO	28.9	1.6	7.5	12.6	48.2	2.5	0.6	21.5	5.5
Ni/MgO	43.9	9.0	33.5	40.5	11.7	0.0	0.0	5.2	0.0
ZrO_2	35.6	7.0	18.7	19.7	32.9	10.4	3.8	7.0	0.7
Ni/ZrO_2	51.3	10.3	36.8	50.2	2.1	0.6	0.0	0.0	0.0
TiO_2	32.8	2.0	12.6	13.7	29.0	17.2	4.1	12.8	7.6
Ni/TiO_2	50.8	13.7	32.6	50.2	2.0	1.4	0.0	0.0	0.0
Al_2O_3	29.5	3.0	8.6	14.6	17.8	43.8	11.8	0.0	0.0
Ni/Al_2O_3	47.5	14.2	29.1	42.9	3.1	9.0	1.2	0.0	0.0
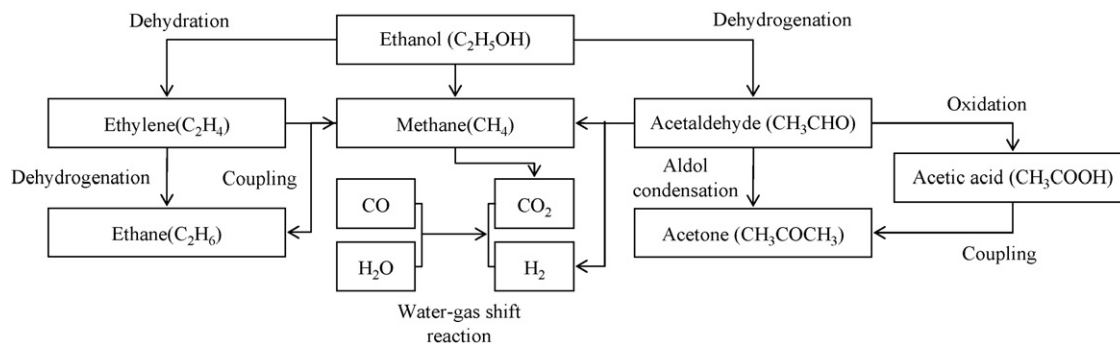
Fig. 3. Reaction pathways in the auto-thermal reforming of ethanol.

in the auto-thermal reforming of ethanol. As presented in Fig. 3, strong/high acidity of support accelerates dehydration of ethanol to form ethylene. On the support with weak/low acidity such as MgO and ZnO, however, dehydrogenation of ethanol to acetaldehyde occurs dominantly.
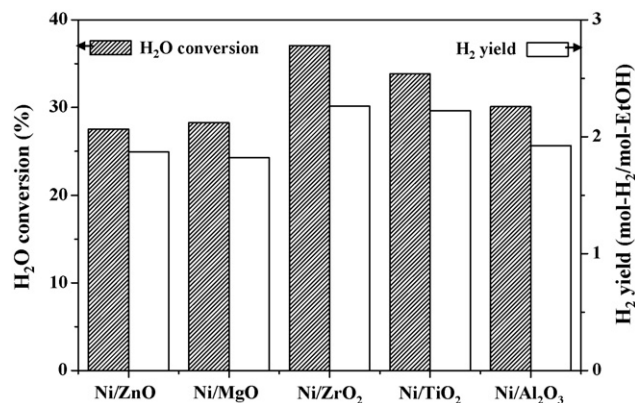
When nickel was supported on pure metal oxide, major products shifted from C_2–C_3 compounds (CH_3CHO, C_2H_4, C_2H_6, CH_3COCH_3, and CH_3COOH) to C_1 compounds (CO, CO_2, and CH_4) and hydrogen. As mentioned earlier (Fig. 2), supported nickel catalyst was more effective for ethanol and water conversions than metal oxide support. This result suggests that nickel played an important role in the C–C bond cleavage and water activation. This result is well consistent with the previous work [30] reporting that nickel activated organic molecules and promoted reaction between adsorbed CH_xO_y fragments and OH groups formed on the support.

Fig. 4 shows the H_2O conversion and H_2 yield over nickel catalysts supported on various pure metal oxides in the auto-thermal

reforming of ethanol. H_2 yield increased with increasing water conversion. This result indicates that the degree of water participation in the reaction is closely related to hydrogen production. It was observed that Ni/ZrO_2 and Ni/TiO_2 catalysts with an intermediate acidity of support exhibited an excellent catalytic performance (H_2 yield). Therefore, ZrO_2 and TiO_2 showing high water conversion (Fig. 2(b)) and hydrogen selectivity (Table 2) could be chosen as efficient supporting materials for nickel catalyst in the auto-thermal reforming of ethanol for hydrogen production.

3.3. Physicochemical properties of $Ti_XZr_{1-X}O_2$ (X = 0, 0.2, 0.5, 0.8, and 1) supports

On the basis of results for pure metal oxide supports, a series of TiO_2–ZrO_2 mixed metal oxides ($Ti_XZr_{1-X}O_2$) with different Ti content (X) were prepared by a sol–gel method with an aim of finding an optimal composition of TiO_2–ZrO_2 for hydrogen production. Table 3 shows the chemical composition, BET surface area, and acidity of $Ti_XZr_{1-X}O_2$ (X = 0, 0.2, 0.5, 0.8, and 1) supports. Chemical composition (atomic ratio) of $Ti_XZr_{1-X}O_2$ (X = 0, 0.2, 0.5, 0.8, and 1) supports was in good agreement with the theoretical value, indicating successful preparation of $Ti_XZr_{1-X}O_2$ (X = 0, 0.2, 0.5, 0.8, and 1) mixed metal oxides. Surface areas of $Ti_0Zr_1O_2$ and

Fig. 4. H_2O conversion and H_2 yield over nickel catalysts supported on various pure metal oxides.

Table 3
Chemical composition, BET surface area, and acidity of $Ti_XZr_{1-X}O_2$ (X = 0, 0.2, 0.5, 0.8, and 1) supports.

Support	Atomic ratio		BET surface area (m^2/g)	Acidity (μmol-NH_3/g)
	Zr	Ti		
$Ti_0Zr_1O_2$	1	0	56	435.2
$Ti_{0.2}Zr_{0.8}O_2$	0.82	0.18	72	859.8
$Ti_{0.5}Zr_{0.5}O_2$	0.52	0.48	137	2368.9
$Ti_{0.8}Zr_{0.2}O_2$	0.21	0.79	80	1234.0
$Ti_1Zr_0O_2$	0	1	43	250.9

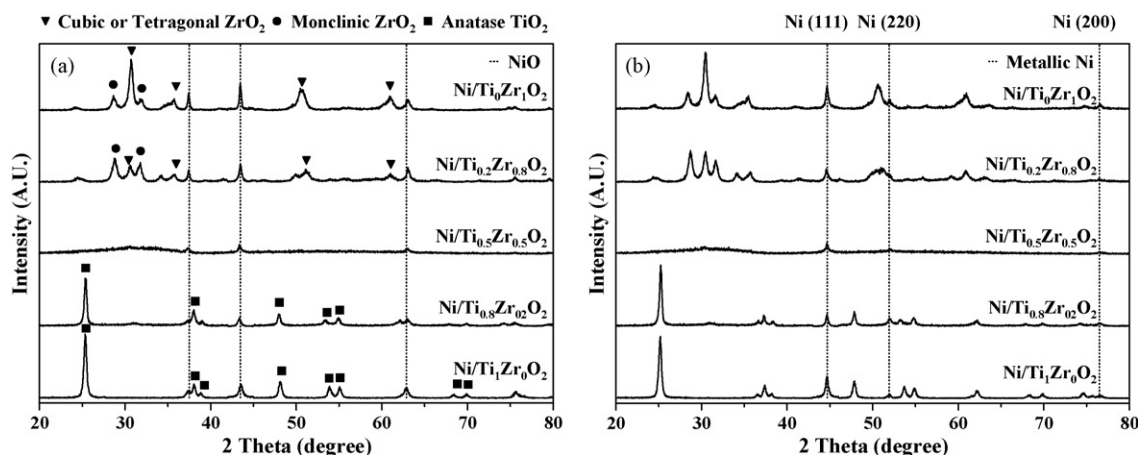**Fig. 5.** XRD patterns of Ni/Ti$_X$Zr$_{1-X}$O$_2$ (X = 0, 0.2, 0.5, 0.8, and 1) catalysts (a) calcined at 550 °C and (b) reduced at 500 °C.

Ti$_1$Zr$_0$O$_2$ were 56 and 43 m^2/g, respectively. However, surface areas of Ti$_X$Zr$_{1-X}$O$_2$ (X = 0.2, 0.5, and 0.8) supports were higher than those of single component metal oxide (Ti$_0$Zr$_1$O$_2$ and Ti$_1$Zr$_0$O$_2$). Among Ti$_X$Zr$_{1-X}$O$_2$ (X = 0, 0.2, 0.5, 0.8, and 1) mixed metal oxide supports, Ti$_{0.5}$Zr$_{0.5}$O$_2$ exhibited the highest surface area. This result can be understood by the fact that surface area of TiO$_2$–ZrO$_2$ binary oxide increased remarkably compared to pure zirconia (Ti$_0$Zr$_1$O$_2$) and titania (Ti$_1$Zr$_0$O$_2$) because degree of crystallization of mixed metal oxide was lower than that of pure metal oxide [31–34].

3.4. Crystal structures of Ni/Ti$_X$Zr$_{1-X}$O$_2$ (X = 0, 0.2, 0.5, 0.8, and 1) catalysts

Fig. 5(a) shows the XRD patterns of Ni/Ti$_X$Zr$_{1-X}$O$_2$ (X = 0, 0.2, 0.5, 0.8, and 1) catalysts calcined at 550 °C. In the Ni/Ti$_0$Zr$_1$O$_2$ catalyst, XRD peaks representing cubic or tetragonal ZrO$_2$ (JCPDS 77-2119 or 27-0997) were dominantly observed at 2θ = 30.7° and 50.6°, and relatively weak peaks indicative of monoclinic ZrO$_2$ (JCPDS 27-0997) and nickel oxide (JCPDS 27-0997) were found. In the Ni/Ti$_{0.2}$Zr$_{0.8}$O$_2$ catalyst, however, XRD peak intensities for cubic or tetragonal ZrO$_2$ decreased together with the decrease of overall crystallinity. In particular, Ni/Ti$_{0.5}$Zr$_{0.5}$O$_2$ catalyst exhibited an amorphous nature. This result is in good agreement with the previous work [33] reporting that a mixed metal oxide of TiO$_2$–ZrO$_2$ (1:1) showed an amorphous feature. It can be inferred that the effect of competitive crystalline growth in the 1:1 binary metal oxide system occurred in the Ni/Ti$_{0.5}$Zr$_{0.5}$O$_2$ catalyst. In other words, the growth of grain sizes of titanium and zirconium oxide species was

inhibited by the presence of Zr^{4+} and Ti^{4+}, respectively [35]. On the other hand, anatase phase of titania was gradually developed in the Ni/Ti$_X$Zr$_{1-X}$O$_2$ (X = 0.8 and 1).

Fig. 5(b) shows the XRD patterns of Ni/Ti$_X$Zr$_{1-X}$O$_2$ (X = 0, 0.2, 0.5, 0.8, and 1) catalysts reduced at 500 °C. Compared to the calcined catalysts (Fig. 5(a)), all the reduced Ni/Ti$_X$Zr$_{1-X}$O$_2$ (X = 0, 0.2, 0.5, 0.8, and 1) catalysts showed narrow XRD peaks for metallic nickel, indicating that nickel oxide was transformed into metallic nickel after the reduction. Crystal size of nickel species in the Ni/Ti$_X$Zr$_{1-X}$O$_2$ catalysts calculated by the Scherrer equation increased in order of Ni/Ti$_{0.5}$Zr$_{0.5}$O$_2$ (13 nm) < Ni/Ti$_{0.8}$Zr$_{0.2}$O$_2$ (17 nm) < Ni/Ti$_{0.2}$Zr$_{0.8}$O$_2$ (19 nm) < Ni/Ti$_0$Zr$_1$O$_2$ (25 nm) ≈ Ni/Ti$_1$Zr$_0$O$_2$ (25 nm), in good agreement with the trend of surface area of Ti$_X$Zr$_{1-X}$O$_2$ support. It can be inferred that the grain size of nickel species was affected by the surface area of supporting materials (Table 3). The dispersion of nickel species in the reduced catalysts was further confirmed by TEM analyses. Fig. 6 shows the TEM images of Ni/Ti$_0$Zr$_1$O$_2$ and Ni/Ti$_{0.5}$Zr$_{0.5}$O$_2$ catalysts. This result also supports that the supported Ni catalyst with large surface area of support showed small particle size and high dispersion of nickel species.

3.5. Acidity of Ti$_X$Zr$_{1-X}$O$_2$ (X = 0, 0.2, 0.5, 0.8, and 1) supports

Fig. 7 shows the NH$_3$-TPD profiles of Ti$_X$Zr$_{1-X}$O$_2$ (X = 0, 0.2, 0.5, 0.8, and 1) supports. Acidity of Ti$_X$Zr$_{1-X}$O$_2$ (X = 0, 0.2, 0.5, 0.8, and 1) supports determined from TPD peak area is summarized in Table 3. It was observed that both surface area and acidity of Ti$_X$Zr$_{1-X}$O$_2$ (X = 0.2, 0.5, and 0.8) supports were much larger
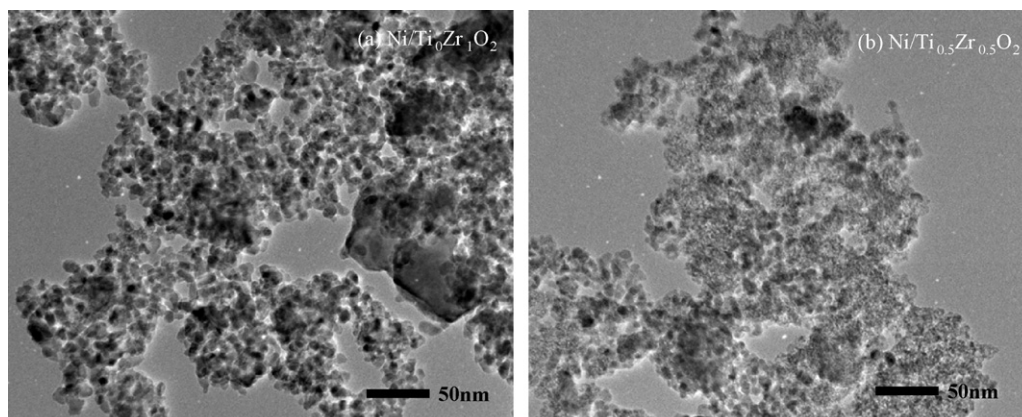

Fig. 6. TEM images of (a) Ni/Ti$_0$Zr$_1$O$_2$ and (b) Ni/Ti$_{0.5}$Zr$_{0.5}$O$_2$ catalysts reduced at 500 °C for 2 h.

Fig. 7. NH_3-TPD profiles of $Ti_XZr_{1-X}O_2$ ($X = 0$, 0.2, 0.5, 0.8, and 1) supports.

Fig. 9. Hydrogen selectivity with time on stream in the auto-thermal reforming of ethanol over $Ni/Ti_XZr_{1-X}O_2$ ($X = 0$, 0.2, 0.5, 0.8, and 1) catalysts at 500 °C. All the catalysts were reduced at 500 °C prior to the reaction.

than those of pure zirconia ($Ti_0Zr_1O_2$) and titania ($Ti_1Zr_0O_2$). It is known that the enhanced acidity of $Ti_XZr_{1-X}O_2$ ($X = 0.2$, 0.5, and 0.8) supports was attributed to charge imbalance in the generation of Ti–O–Zr bonding [36,37]. Among the supports examined, $Ti_{0.5}Zr_{0.5}O_2$ exhibited the largest surface area (137 m^2/g) and acidity (2369.8 μmol-NH_3/g).

3.6. TPR behavior of $Ni/Ti_XZr_{1-X}O_2$ ($X = 0$, 0.2, 0.5, 0.8, and 1) catalysts

TPR measurements were carried out to investigate the reducibility of $Ni/Ti_XZr_{1-X}O_2$ ($X = 0$, 0.2, 0.5, 0.8, and 1) catalysts and to see the interaction between nickel and support. Fig. 8 shows the TPR profiles of $Ni/Ti_XZr_{1-X}O_2$ ($X = 0$, 0.2, 0.5, 0.8, and 1) catalysts. It is known that unsupported NiO is reduced at around 280 °C [38]. However, no peaks related to the reduction of bulk NiO were found in the $Ni/Ti_XZr_{1-X}O_2$ ($X = 0$, 0.2, 0.5, 0.8, and 1) catalysts. In the $Ni/Ti_0Zr_1O_2$ catalyst, one reduction peak attributed to the reduction of NiO interacted with Ti_0ZrO_2 was observed at around 450 °C [39]. In the $Ni/Ti_1Zr_0O_2$ catalyst, on the other hand, one reduction peak attributed to the reduction of NiO interacted with $Ti_1Zr_0O_2$ was observed at around 570 °C. Upon metal substitution in the $Ti_XZr_{1-X}O_2$ ($X = 0.2$, 0.5, and 0.8), however, broad reduction peaks appeared within the temperature range of 400–700 °C, indicating the formation of nickel species with differ-

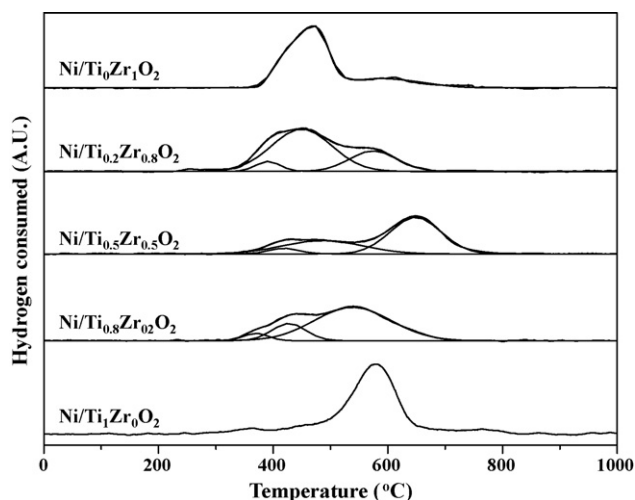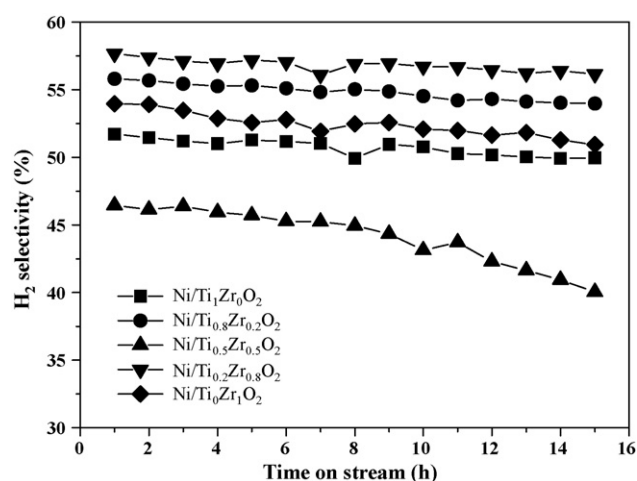ent oxidation states. According to the literature [40], metal sites became more electron deficient due to the interaction between metal species and acid sites of the support with increasing acidity. Major part of these acid sites serves as an electron acceptor (Lewis acid) [32,33], resulting in the formation of many electron deficient sites in the TiO_2–ZrO_2 mixed metal oxide supports [41,42]. Therefore, it can be inferred that the enhanced support acidity in the $Ti_XZr_{1-X}O_2$ ($X = 0.2$, 0.5, and 0.8) supports leads to an enhancement of electron deficient sites in the $Ni/Ti_XZr_{1-X}O_2$ ($X = 0.2$, 0.5, and 0.8) catalysts, resulting in the formation of nickel species with different oxidation states. Among the $Ni/Ti_XZr_{1-X}O_2$ ($X = 0$, 0.2, 0.5, 0.8, and 1) catalysts, $Ni/Ti_{0.5}Zr_{0.5}O_2$ with the strongest support acidity showed the strongest metal–support interaction and the highest metal dispersion (the smallest nickel crystal size) due to the formation of large amount of electron deficient sites on the $Ti_{0.5}Zr_{0.5}O_2$ support. These characteristics of TiO_2–ZrO_2 mixed metal oxide supports may affect the crystal size and dispersion of nickel species in the $Ni/Ti_XZr_{1-X}O_2$ catalysts. However, $Ni/Ti_{0.2}Zr_{0.8}O_2$ and $Ni/Ti_{0.8}Zr_{0.2}O_2$ catalysts with partial metal substitution formed more reducible nickel species and retained higher nickel dispersion than $Ni/Ti_0Zr_1O_2$ and $Ni/Ti_1Zr_0O_2$, respectively. In particular, $Ni/Ti_{0.2}Zr_{0.8}O_2$ catalyst exhibited the highest reducibility (the lowest reduction peak temperature).

3.7. Catalytic performance of $Ni/Ti_XZr_{1-X}O_2$ ($X = 0$, 0.2, 0.5, 0.8, and 1) catalysts

All the $Ni/Ti_XZr_{1-X}O_2$ ($X = 0$, 0.2, 0.5, 0.8, and 1) catalysts tested in this work exhibited complete conversion of ethanol at 500 °C, while product distributions over the catalysts were different depending on the support composition. Fig. 9 shows the hydrogen selectivity with time on stream in the auto-thermal reforming of ethanol over $Ni/Ti_XZr_{1-X}O_2$ ($X = 0$, 0.2, 0.5, 0.8, and 1) catalysts at 500 °C. Hydrogen selectivity decreased in the order of $Ni/Ti_{0.2}Zr_{0.8}O_2 > Ni/Ti_{0.8}Zr_{0.2}O_2 > Ni/Ti_0Zr_1O_2 > Ni/Ti_1Zr_0O_2 > Ni/Ti_{0.5}Zr_{0.5}O_2$. $Ni/Ti_{0.2}Zr_{0.8}O_2$ catalyst with small amount of titanium substitution not only formed easily reducible nickel species but also retained high nickel dispersion than $Ni/Ti_0Zr_1O_2$ catalyst. Likewise, the enhanced catalytic performance of $Ni/Ti_{0.8}Zr_{0.2}O_2$ catalyst compared to $Ni/Ti_1Zr_0O_2$ was also attributed to the formation of reducible nickel species and the enhancement of nickel dispersion. In case of $Ni/Ti_{0.5}Zr_{0.5}O_2$ catalyst, however, hydrogen selectivity was very low and steadily decreased with time on stream. This suggests that $Ni/Ti_{0.5}Zr_{0.5}O_2$ catalyst becomes

Fig. 8. TPR profiles of $Ni/Ti_XZr_{1-X}O_2$ ($X = 0$, 0.2, 0.5, 0.8, and 1) catalysts.
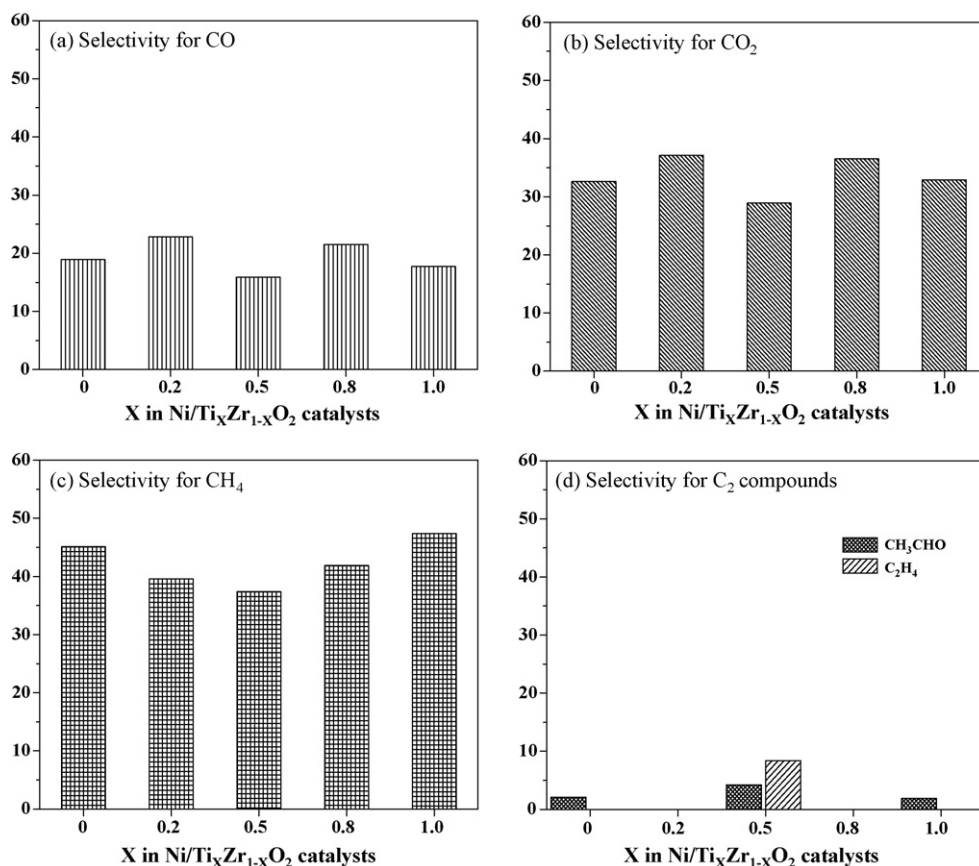
Fig. 10. By-product selectivity in the auto-thermal reforming of ethanol over $Ni/Ti_XZr_{1-X}O_2$ ($X = 0$, 0.2, 0.5, 0.8, and 1) catalysts at 500 °C: (a) selectivity for CO, (b) selectivity for CO_2, (c) selectivity for CH_4, and (d) selectivity for C_2 compounds (C_2H_4 and CH_3CHO). Reaction data were obtained after a 15 h reaction.

deactivated via the boudouard reaction ($2CO \rightarrow CO_2 + C$) and ethylene pyrolysis coking formation ($C_2H_4 \rightarrow polymer \rightarrow coke$) due to strong/high acidity of $Ti_{0.5}Zr_{0.5}O_2$ support [43–45].

To elucidate the effect of Ti content (X) on the product distribution over $Ni/Ti_XZr_{1-X}O_2$ ($X = 0$, 0.2, 0.5, 0.8, and 1) catalysts, selectivity for by-products such as CO, CO_2, CH_4, and C_2 compounds (C_2H_4 and CH_3CHO) was measured as shown in Fig. 10. In the $Ni/Ti_{0.2}Zr_{0.8}O_2$ and $Ni/Ti_{0.8}Zr_{0.2}O_2$ catalysts, acetaldehyde steam reforming reaction ($CH_3CHO + H_2O \rightarrow H_2 + CO_2 + CH_4$) and methane steam reforming reaction ($CH_4 + H_2O \rightarrow 3H_2 + CO$) occurred, resulting in an increase of selectivity for H_2, CO, and CO_2, and a decrease of selectivity for CH_4 and C_2 compounds. It is noteworthy that formation of C_2H_4 was mainly observed over $Ni/Ti_{0.5}Zr_{0.5}O_2$ catalysts because of strong/high acidity of $Ti_{0.5}Zr_{0.5}O_2$ support. On the other hand, selectivity for CO_2 and CH_4, which were formed via the reaction of $C_2H_5OH + H_2O \rightarrow CH_4 + CO_2 + 2H_2$, was much higher than that for CO, C_2H_4, and CH_3CHO over $Ni/Ti_XZr_{1-X}O_2$ ($X = 0$, 0.2, 0.5, 0.8, and 1) catalysts. Furthermore, selectivity for CO_2 and CO over $Ni/Ti_XZr_{1-X}O_2$ ($X = 0$, 0.2, 0.5, 0.8, and 1) catalysts showed a similar trend to that for hydrogen (Fig. 9).

3.8. Effect of support acidity on catalytic performance over supported nickel catalysts

Fig. 11 shows the correlation between acidity of supports and hydrogen yield over supported nickel catalysts in the auto-thermal reforming of ethanol, established for all supported nickel catalysts examined in this work. It should be noted that hydrogen yield over supported nickel catalysts showed a volcano-shaped curve with respect to acidity of the support. This result indicates that an optimal acidity is required for maximum yield of hydro-

gen. Maximum hydrogen yield observed for $Ni/Ti_{0.2}Zr_{0.8}O_2$ was ca. 2.6 mol-H_2/mol-EtOH. Although this value was lower than the theoretical value (ca. 6.0 mol-H_2/mol-EtOH), it was a little higher than the reported value [46–48]. It is concluded that surface area and acidity of pure zirconia and titania could be modified by forming ZrO_2–TiO_2 mixed metal oxide. $Ti_{0.2}Zr_{0.8}O_2$ and $Ti_{0.8}Zr_{0.2}O_2$ supports with partial metal substitution favorably served as supporting materials for improving nickel dispersion and reducibility of the
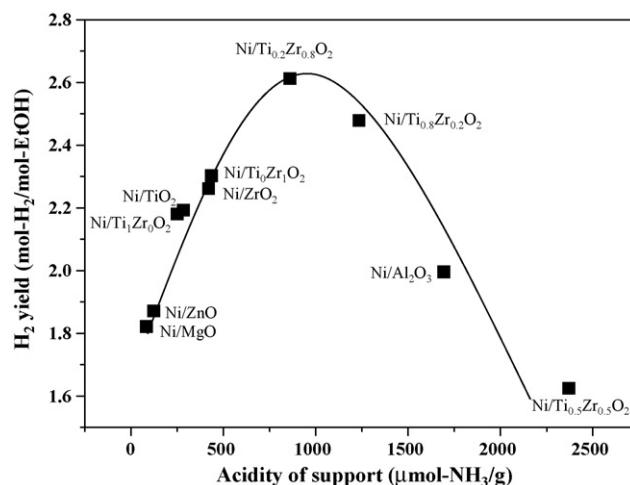
Fig. 11. A correlation between acidity of supports and hydrogen yield over supported nickel catalysts in the auto-thermal reforming of ethanol, established for all supported nickel catalysts examined in this work. Reaction data were obtained after a 15 h reaction.

catalysts, leading to an enhanced catalytic performance. In the case of $Ti_{0.5}Zr_{0.5}O_2$ support, however, strong/high acidity caused by charge imbalance in the generation of Ti–O–Zr bonding induced small nickel particles, leading to poor reducibility and low catalytic performance of supported nickel catalyst.

4. Conclusions

Nickel catalysts supported on pure metal oxides (ZnO, MgO, ZrO_2, TiO_2, and Al_2O_3) with different acidity were prepared by an incipient wetness impregnation method, and they were applied to the hydrogen production by auto-thermal reforming of ethanol. Among various pure metal oxides, ZrO_2 and TiO_2 with an intermediate acidity were found to be efficient supports for nickel catalysts in hydrogen production by auto-thermal reforming of ethanol. On the basis of this result, a series of $Ti_XZr_{1-X}O_2$ mixed metal oxides with different Ti content were prepared by a sol–gel method with an attempt to find an optimal composition of TiO_2–ZrO_2 for hydrogen production. Nickel catalysts supported on $Ti_XZr_{1-X}O_2$ ($X = 0$, 0.2, 0.5, 0.8, and 1) were then prepared by an incipient wetness impregnation method, and they were applied to hydrogen production by auto-thermal reforming of ethanol. A correlation between hydrogen yield over supported nickel catalysts and acidity of supports revealed that hydrogen yield over the catalysts showed a volcano-shaped curve with respect to acidity of the support. Among the catalysts tested, $Ni/Ti_{0.2}Zr_{0.8}O_2$ with an intermediate acidity of support exhibited the best catalytic performance. Thus, acidity of support served as an important factor determining the catalytic performance of supported nickel catalysts in hydrogen production by auto-thermal reforming of ethanol.

Acknowledgement

References

[1] M. Schrope, Nature 414 (2001) 682–684.
[2] W. Seifritz, Int. J. Hydrogen Energy 30 (2005) 45–51.
[3] P. Moriarty, D. Honnery, Int. J. Hydrogen Energy 32 (2007) 1616–1624.
[4] T.A. Semelsberger, K.C. Ott, R.L. Borup, H.L. Greene, Appl. Catal. B 65 (2006) 291–300.
[5] D.K. Liguras, D.I. Kondarides, X.E. Verykios, Appl. Catal. B 43 (2003) 345–354.
[6] A.N. Fatsikostas, D.I. Kondarides, X.E. Verykios, Catal. Today 75 (2002) 145–155.
[7] N. Meng, D.Y.C. Leung, M.K.H. Leung, Int. J. Hydrogen Energy 32 (2007) 3238–3247.
[8] G. Rabenstein, V. Hacker, J. Power Sources 185 (2008) 1293–1304.
[9] M.H. Youn, J.G. Seo, P. Kim, J.J. Kim, H.-I. Lee, I.K. Song, J. Power Sources 162 (2006) 1270–1274.
[10] N. Laosiripojana, S. Assabumrungrat, S. Charojrochkul, Appl. Catal. A 327 (2007) 180–188.
[11] P. Biswas, D. Kunzru, Chem. Eng. J. 136 (2008) 41–49.
[12] J. Kugai, V. Subramani, C. Song, M.H. Engelhard, Y.-H. Chin, J. Catal. 238 (2006) 430–440.
[13] F. Frusteri, S. Freni, V. Chiodo, S. Donato, G. Bonura, S. Cavallaro, Int. J. Hydrogen Energy 31 (2006) 2193–2199.
[14] M.H. Youn, J.G. Seo, J.C. Jung, S. Park, D.R. Park, S.-B. Lee, I.K. Song, Catal. Today 146 (2009) 57–62.
[15] M.H. Youn, J.G. Seo, P. Kim, I.K. Song, J. Mol. Catal. A 261 (2007) 276–281.
[16] J.G. Seo, M.H. Youn, K.M. Cho, S. Park, S.H. Lee, J. Lee, I.K. Song, Korean J. Chem. Eng. 25 (2008) 41–45.
[17] P. Biswas, D. Kunzru, Int. J. Hydrogen Energy 32 (2007) 969–980.
[18] S. Wang, G.Q.M. Lu, Appl. Catal. B 16 (1998) 269–277.
[19] G.B. Sun, K. Hidajat, X.S. Wu, S. Kawi, Appl. Catal. B 81 (2008) 303–312.
[20] A.C. Furtado, C.G. Alonso, M.P. Cantão, N.R.C. Fernandes-Machado, Int. J. Hydrogen Energy 34 (2009) 7189–7196.
[21] M.C. Sánchez-Sánchez, R.M. Navarro, J.L.G. Fierro, Int. J. Hydrogen Energy 32 (2007) 1462–1471.
[22] M.H. Youn, J.G. Seo, K.M. Cho, J.C. Jung, H. Kim, K.W. La, D.R. Park, S. Park, S.H. Lee, I.K. Song, Korean J. Chem. Eng. 25 (2008) 236–238.
[23] Y. Yang, J. Ma, F. Wu, Int. J. Hydrogen Energy 31 (2006) 877–882.
[24] J. Zhang, J. Chen, J. Ren, Y. Li, Y. Sun, Fuel 82 (2003) 581–586.
[25] V. Bolis, C. Morterra, M. Volante, L. Orio, B. Fubini, Langmuir 6 (1990) 695–701.
[26] H. Yamashita, Y. Nishida, S. Yuan, K. Mori, M. Narisawa, Y. Matsumura, T. Ohmichi, I. Katayama, Catal. Today 120 (2007) 163–167.
[27] A.L. Linsebigler, G. Lu, J.T. Yates, Chem. Rev. 95 (1995) 735–758.
[28] Y. Matsumura, T. Nakamori, Appl. Catal. A 258 (2004) 107–114.
[29] J.G. Seo, M.H. Youn, S. Park, J. Lee, S.H. Lee, H. Lee, I.K. Song, Korean J. Chem. Eng. 25 (2008) 95–98.
[30] S.M. Gates, J.N. Russell, J.T. Yates, Surf. Sci. 171 (1986) 111–134.
[31] H. Zou, Y.S. Lin, Appl. Catal. A 265 (2004) 35–42.
[32] J.R. Sohn, S.H. Lee, Appl. Catal. A 321 (2007) 27–34.
[33] M.E. Manríquez, T. López, R. Gómez, J. Navarrete, J. Mol. Catal. A 220 (2004) 229–237.
[34] M. Laniecki, M. Ignacik, Catal. Today 116 (2006) 400–407.
[35] Y.M. Wang, S.W. Liu, M.K. Lu, S.F. Wang, F. Gu, X.Z. Gai, X.P. Cui, J. Pan, J. Mol. Catal. A 215 (2004) 137–142.
[36] J.C. Yu, J. Lin, R.W.M. Kwok, J. Phys. Chem. B 102 (1998) 5094–5098.
[37] J.C. Wu, C.S. Chung, C.L. Ay, I. Wang, J. Catal. 87 (1984) 98–107.
[38] T. Wu, Q. Yan, H. Wan, J. Mol. Catal. A 226 (2005) 41–48.
[39] S. Xu, X. Wang, Fuel 84 (2005) 563–567.
[40] A.Y. Stakheev, L.M. Kustov, Appl. Catal. A 188 (1999) 3–35.
[41] B.M. Reddy, B. Chowdhurya, P.G. Smirniotis, Appl. Catal. A 211 (2001) 19–30.
[42] B.M. Reddy, P.M. Sreekantha, Y. Yamadab, Q. Xub, T. Kobayashi, Appl. Catal. A 228 (2002) 269–278.
[43] A.N. Fatsikostas, X.E. Verykios, J. Catal. 25 (2004) 439–452.
[44] S. Freni, S. Cavallarob, N. Mondelloa, L. Spadaroa, F. Frusteri, Catal. Commun. 4 (2003) 259–268.
[45] H. Nakano, J. Ogawa, J. Nakamura, Surf. Sci. 514 (2002) 256–260.
[46] J. Sun, Y. Wang, J. Li, G. Xiao, L. Zhang, H. Li, Y. Cheng, C. Sun, Z. Cheng, Z. Dong, L. Chen, Int. J. Hydrogen Energy 35 (2010) 3087–3091.
[47] L.P.R. Profeti, J.A.C. Dias, J.M. Assaf, E.M. Assaf, J. Power Sources 190 (2009) 525–533.
[48] L.P.R. Profeti, E.A. Ticianelli, E.M. Assaf, Int. J. Hydrogen Energy 34 (2009) 5049–5060.